A priori estimates on the partial realized gain of UWB-antennas

Sohl, Christian; Gustafsson, Mats

2007

CODEN:LUTEDX/(TEAT-7160)/1-19/(2007)

A priori estimates on the partial realized gain of UWB-antennas

Christian Sohl and Mats Gustafsson

Electromagnetic Theory
Department of Electrical and Information Technology
Lund University
Sweden

Christian Sohl and Mats Gustafsson
{Christian.Sohl,Mats.Gustafsson}@eit.lth.se

Department of Electrical and Information Technology
Electromagnetic Theory
P.O. Box 118
SE-221 00 Lund
Sweden

Editor: Gerhard Kristensson

Abstract

A summation rule or dispersion relation valid for any causal and reciprocal antenna is presented in terms of the electric and magnetic polarizability dyadics. The identity is based on the holomorphic properties of the forward scattering dyadic and includes arbitrary shaped antennas modeled by linear and time-translational invariant constitutive relations. In particular, a priori estimates on the partial realized gain are introduced, and lower bounds on the onset frequency is derived for two important archetypes of UWB-antennas. The theoretical findings are illustrated by the equiangular planar spiral antenna, and comparison with numerical simulations show great potential for future applications in antenna theory.

1 Introduction

Since the pioneering ideas introduced by Chu and Wheeler in Refs. 3 and 23 more than half a century ago, a priori bounds on the directivity and the Q-factor of electrically small antennas have attracted great attention in the scientific community. Unfortunately, the results by Chu and Wheeler, and many of the subsequent papers discussed in Ref. 9, not only overestimate the true antenna performance, but also show severe restrictions such as the lack of any material description and polarization dependence. To overcome these imperfections, a new set of isoperimetric bounds are introduced in Refs. 6 and 8 that apply to a large class of linear and reciprocal antennas. These new bounds are based on the first principles of primitive causality and power conservation rather than the traditional approach of the spherical vector waves. Another drawback of the classical formulation is due to the difficulty of extending the spherical vector waves to accurately model the electromagnetic field inside the smallest circumscribing sphere. As a consequence, the estimates in this paper apply to antennas of arbitrary shape without introducing the misleading concept of the smallest circumscribing sphere.

The classical bounds summarized in Ref. 9 also show severe restrictions with respect to the electrical size and frequency characteristic of the antenna. In particular, the classical bounds are only meaningful for electrically small and resonant antennas due to the underlying assumption of a dominant lowest order spherical vector mode. As far as the authors know, no similar bounds to Chu and Wheeler exist in the literature for non-resonant antennas with a broadband partial realized gain. An exception is given by Refs. 10 and 22 which address limitations on the bandwidth using Fano's theory of broadband matching. Since non-resonant antennas show great potential in future communication technologies such as Ultra-Wideband (UWB), it is of scientific importance to establish a priori estimates to quantify the tradeoff between the antenna onset frequency and its partial realized gain.

The underlying idea of UWB-systems is the spreading of the transmitted data over an absolute bandwidth exceeding the lesser of 500 MHz or 20% of the center frequency, see pp. 30–33 in Ref. 15.[1] The UWB-system uses a low power spectral

[1] For example, in North America, $[3.1, 10.6]$ GHz is authorized by the Federal Communications

density for short-range communication, implying that frequency bands already assigned to other services can be re-used in a cooperative manner without introducing significant interference. Among other things, UWB-antennas show great potential for applications in stealth technology, radar imaging and precision positioning. In the above-mentioned applications, an undesired feature of many UWB-antennas is the presence of temporal dispersion, *i.e.*, the stretching of a time-domain signal into a more distorted waveform, in the sense that the phase center or effective origin of the radiated field varies with frequency. This variation is due to the fact that small-scale portions of the antenna radiate or receive high-frequency components, and large-scale portions radiate or receive low-frequency components. The present paper does not further address the problem of temporal dispersion and its effect on the antenna performance. Neither does it discuss how to minimize the temporal dispersion associated with a radiation pattern that varies with frequency.

The bounds presented in this paper follow Ref. 7 by picturing the antenna from a scattering point of view using the formalism in Refs. 2 and 14. Specifically, the holomorphic properties of the forward scattering dyadic is employed in Refs. 17 and 18 to derive a summation rule for the extinction cross section. In Ref. 6, this identity is carried over from the scattering scenario to a large class of antennas via the effective antenna aperture. In particular, the variational results derived by Jones in Refs. 11 and 12 play an essential role for the far reaching conclusions that is established from this new theory. However, the main importance of the theoretical findings is that they directly can be invoked in antenna design to provide knowledge of the tradeoff between the partial realized gain and the bandwidth present in a given structure. The results are also crucial for the understanding of the physical effects imposed on any antenna by the first principles of primitive causality and power conservation.

2 The integrated partial realized gain

Consider a linear, lossless and reciprocal antenna embedded in free space as depicted in Fig. 1.[2] The assumption of a reciprocal material means that either the transmission case or the reception case may be examined. From a scattering point of view, the antenna is assumed to satisfy primitive causality in the sense of pp. 17–22 in Ref. 20, *viz.*, the scattered field in the forward direction cannot precede the incident field when subject to a plane wave excitation. Let $\hat{\boldsymbol{k}}$ denote a fixed direction in space, and consider a radiated field with an electric polarization $\hat{\boldsymbol{e}}$ satisfying $\hat{\boldsymbol{e}} \cdot \hat{\boldsymbol{k}} = 0$ in the far field region. Introduce the partial realized gain g as a measure of the antenna's ability to direct or focus energy. It is defined as the partial gain G in the $\hat{\boldsymbol{k}}$-direction with respect to the $\hat{\boldsymbol{e}}$-polarization, weighted with the reflection loss due to the antenna mismatch (Γ denotes the reflection coefficient at the antenna

Commission (FCC) as the appropriate frequency band for UWB-communication.

[2]The assumption of a lossless material is not a serious restriction since it can be relaxed by including an ohmic efficiency in (2.1) and the subsequent analysis.

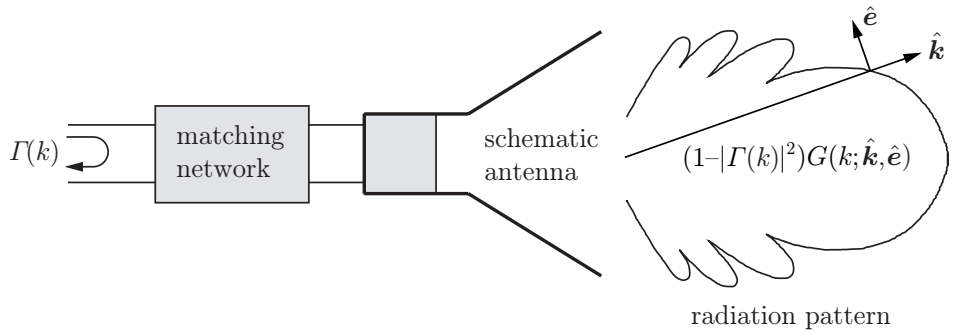

Figure 1: The radiation pattern of a schematic antenna in terms of the partial realized gain.

port), *i.e.*,

$$g(k;\hat{\boldsymbol{k}},\hat{\boldsymbol{e}}) = (1-|\Gamma(k)|^2)G(k;\hat{\boldsymbol{k}},\hat{\boldsymbol{e}}), \tag{2.1}$$

where $\hat{\boldsymbol{k}}$ and $\hat{\boldsymbol{e}}$ are independent of the wave number $k \in [0,\infty)$.[3] The definition (2.1) includes both the TE- and TM-polarizations, or any combination thereof.

Based on the above-stated assumptions, a summation rule or dispersion relation known as the integrated partial realized gain is derived in Ref. 6 in terms of the electric and magnetic polarizability dyadics, $\boldsymbol{\gamma}_{\mathrm{e}}$ and $\boldsymbol{\gamma}_{\mathrm{m}}$, respectively. The result is

$$\int_0^\infty \frac{g(k;\hat{\boldsymbol{k}},\hat{\boldsymbol{e}})}{k^4}\,\mathrm{d}k = \frac{\eta(-\hat{\boldsymbol{k}},\hat{\boldsymbol{e}}^*)}{2}\left(\hat{\boldsymbol{e}}^*\cdot\boldsymbol{\gamma}_{\mathrm{e}}\cdot\hat{\boldsymbol{e}} + (\hat{\boldsymbol{k}}\times\hat{\boldsymbol{e}}^*)\cdot\boldsymbol{\gamma}_{\mathrm{m}}\cdot(\hat{\boldsymbol{k}}\times\hat{\boldsymbol{e}})\right), \tag{2.2}$$

where an asterisk denotes the complex conjugate, and the general absorption efficiency $\eta \in [0,1)$ is defined in Sec. 3. Relation (2.2) also holds for non-reciprocal antennas if g is interpreted as the partial realized gain in receiving mode.

The identity (2.2) is valid for a large class of bi-anisotropic and heterogeneous material models including temporal dispersion with or without a conductivity term. Here, the material of the antenna is quantified in terms of the real-valued and symmetric polarizability dyadics, $\boldsymbol{\gamma}_{\mathrm{e}}$ and $\boldsymbol{\gamma}_{\mathrm{m}}$, defined in Sec. 4 by certain electrostatic and magnetostatic boundary value problems. These dyadics depend on the geometry of the antenna and its static material parameters, and they are independent of any matching network. On the other hand, the generalized absorption efficiency η depends on the dynamic properties of the antenna (including the matching network), and it is defined as the ratio of the integrated absorption to the integrated extinction. The generalized absorption efficiency is a real-valued number in the unit interval

[3] According to the IEEE-standard in Ref. 1, the partial gain G in a given direction is defined as "that part of the radiation intensity corresponding to a given polarization divided by the radiation intensity that would be obtained if the power accepted by the antenna were radiated isotropically". In this way, the partial realized gain (2.1) contains more information than the maximum gain,

$$G_{\max}(k) = \max_{\hat{\boldsymbol{k}}\cdot\hat{\boldsymbol{e}}=0} G(k;\hat{\boldsymbol{k}},\hat{\boldsymbol{e}}),$$

which is maximized with respect to both the $\hat{\boldsymbol{k}}$- and $\hat{\boldsymbol{e}}$-directions.

quantifying the overall scattering and absorption properties of the antenna. Based on reciprocity, η is determined from the scattering of a plane wave $\mathrm{e}^{-\mathrm{i}k\hat{\boldsymbol{k}}\cdot\boldsymbol{x}}\hat{\boldsymbol{e}}^*$ of unit amplitude impinging in the $-\hat{\boldsymbol{k}}$-direction, see Sec. 3.

3 Scattering and absorption of antennas

Now, consider the schematic antenna in Fig. 2 subject to a plane wave $\mathrm{e}^{-\mathrm{i}k\hat{\boldsymbol{k}}\cdot\boldsymbol{x}}\hat{\boldsymbol{e}}^*$ of unit amplitude. A collective measure of the antenna's scattering properties is then given by the scattering cross section σ_{s}, defined as the scattered power divided by the incident power flux in the forward direction. A corresponding measure for the absorbed power in the antenna is the effective antenna aperture or absorption cross section σ_{a}. Recall that σ_{a} and σ_{s} are real-valued and non-negative. The latter is determined by integrating the scattering dyadic $\mathbf{S}$ over the unit sphere Ω with respect to $\hat{\boldsymbol{x}} = \boldsymbol{x}/x$, *viz.*,

$$\sigma_{\mathrm{s}}(k; -\hat{\boldsymbol{k}}, \hat{\boldsymbol{e}}^*) = \int_\Omega |\mathbf{S}(k; -\hat{\boldsymbol{k}} \curvearrowright \hat{\boldsymbol{x}}) \cdot \hat{\boldsymbol{e}}^*|^2 \, \mathrm{dS},$$

where the notation $-\hat{\boldsymbol{k}} \curvearrowright \hat{\boldsymbol{x}}$ refers to the scattering of a plane wave incident in the $-\hat{\boldsymbol{k}}$-direction into an outgoing spherical wave in the $\hat{\boldsymbol{x}}$-direction. The scattering dyadic $\mathbf{S}$ is related to the scattered electric field $\boldsymbol{E}_{\mathrm{s}}$ via[4]

$$\mathbf{S}(k; -\hat{\boldsymbol{k}} \curvearrowright \hat{\boldsymbol{x}}) \cdot \hat{\boldsymbol{e}}^* = \lim_{x\to\infty} x\mathrm{e}^{-\mathrm{i}kx} \boldsymbol{E}_{\mathrm{s}}(k, \boldsymbol{x}; -\hat{\boldsymbol{k}}, \hat{\boldsymbol{e}}^*),$$

where $x = |\boldsymbol{x}|$ denotes the magnitude of the position vector. As mentioned in Sec. 2, it is assumed that the configuration in Fig. 2 is primitive causal in the forward direction, $\hat{\boldsymbol{x}} = -\hat{\boldsymbol{k}}$, meaning that the inverse Fourier transform of $\hat{\boldsymbol{e}}\cdot\mathbf{S}(k; -\hat{\boldsymbol{k}} \curvearrowright -\hat{\boldsymbol{k}})\cdot \hat{\boldsymbol{e}}^*$ vanishes on the negative real axis. In fact, the assumption of primitive causality is crucial for establishing the holomorphic properties of $\hat{\boldsymbol{e}} \cdot \mathbf{S}(k; -\hat{\boldsymbol{k}} \curvearrowright -\hat{\boldsymbol{k}}) \cdot \hat{\boldsymbol{e}}^*$ that are used to derive the summation rule (2.2) in Ref. 6.

An antenna's ability to intercept an incident wave is often measured by the effective antenna aperture σ_{a}. In terms of the optical theorem on pp. 18–20 in Ref. 14, the effective antenna aperture is given by

$$\sigma_{\mathrm{a}}(k; -\hat{\boldsymbol{k}}, \hat{\boldsymbol{e}}^*) = \frac{4\pi}{k} \operatorname{Im}\left\{\hat{\boldsymbol{e}} \cdot \mathbf{S}(k, -\hat{\boldsymbol{k}} \curvearrowright -\hat{\boldsymbol{k}}) \cdot \hat{\boldsymbol{e}}^*\right\} - \sigma_{\mathrm{s}}(k; -\hat{\boldsymbol{k}}, \hat{\boldsymbol{e}}^*),$$

implying that the received power in the antenna simply is the product of σ_{a} and the incident power flux. As a consequence of reciprocity, the effective antenna aperture is related to the partial realized gain via, see pp. 177–179 in Ref. 16,

$$\sigma_{\mathrm{a}}(k; -\hat{\boldsymbol{k}}, \hat{\boldsymbol{e}}^*) = \frac{\pi g(k; \hat{\boldsymbol{k}}, \hat{\boldsymbol{e}})}{k^2}. \tag{3.1}$$

[4]Here, $\boldsymbol{E}_{\mathrm{s}} = \boldsymbol{E}_{\mathrm{tot}} - \mathrm{e}^{-\mathrm{i}k\hat{\boldsymbol{k}}\cdot\boldsymbol{x}}\hat{\boldsymbol{e}}^*$, where the total electric field $\boldsymbol{E}_{\mathrm{tot}}$ satisfies the Maxwell equations on pp. 3–4 in Ref. 14.

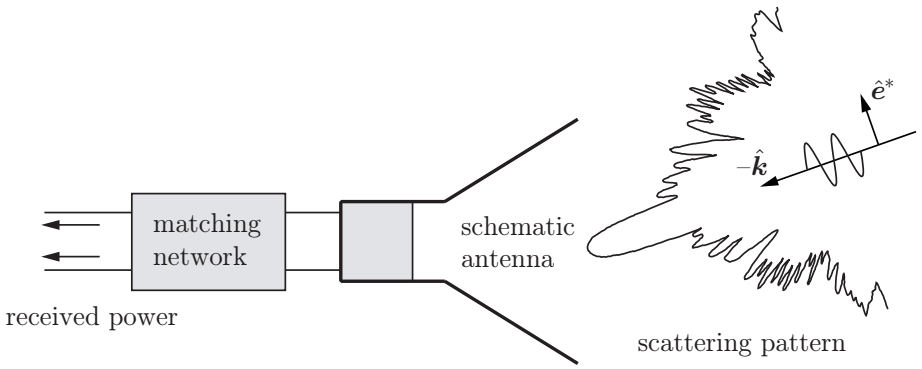

Figure 2: The resulting scattering pattern when the schematic antenna in Fig. 1 is illuminated by a plane wave $\mathrm{e}^{-\mathrm{i}k\hat{\boldsymbol{k}}\cdot\boldsymbol{x}}\hat{\boldsymbol{e}}^*$ of unit amplitude.

Relation (3.1) establishes a connection between an antenna's ability to absorb an incident wave and its property to direct or focus energy.

The generalized absorption efficiency $\eta \in [0,1)$ introduced in Sec. 2 is an overall measure of the scattering and absorption due to the presence of the antenna. Equivalently, it is a quality measure of the choice of location of the feeding port. The generalized absorption efficiency is defined as the ratio between the integrated absorption and the integrated extinction, *i.e.*,

$$\eta(-\hat{\boldsymbol{k}},\hat{\boldsymbol{e}}^*) = \int_0^\infty \frac{\sigma_{\mathrm{a}}(k;-\hat{\boldsymbol{k}},\hat{\boldsymbol{e}}^*)}{k^2}\,\mathrm{d}k \Bigg/ \int_0^\infty \frac{\sigma_{\mathrm{ext}}(k;-\hat{\boldsymbol{k}},\hat{\boldsymbol{e}}^*)}{k^2}\,\mathrm{d}k\,, \tag{3.2}$$

where $\sigma_{\mathrm{ext}} = \sigma_{\mathrm{a}} + \sigma_{\mathrm{s}}$ denotes the extinction cross section. For a large class of antennas, η is close to $1/2$ if $\hat{\boldsymbol{k}}$ and $\hat{\boldsymbol{e}}$ coincide with the antenna's main beam and intrinsic polarization, respectively. The integrated absorption depends on the presence of the matching network in the antenna, and it is determined experimentally by loading the antenna with the appropriate radiation resistance and calculating the absorbed power when the antenna is subject to the plane wave excitation $\mathrm{e}^{-\mathrm{i}k\hat{\boldsymbol{k}}\cdot\boldsymbol{x}}\hat{\boldsymbol{e}}^*$.

According to Ref. 17, the denominator in (3.2) can also be formulated in terms of the electric and magnetic polarizability dyadics, $\boldsymbol{\gamma}_{\mathrm{e}}$ and $\boldsymbol{\gamma}_{\mathrm{m}}$, respectively, *viz.*,

$$\int_0^\infty \frac{\sigma_{\mathrm{ext}}(k;-\hat{\boldsymbol{k}},\hat{\boldsymbol{e}}^*)}{k^2}\,\mathrm{d}k = \frac{\pi}{2}\left(\hat{\boldsymbol{e}}^*\cdot\boldsymbol{\gamma}_{\mathrm{e}}\cdot\hat{\boldsymbol{e}} + (\hat{\boldsymbol{k}}\times\hat{\boldsymbol{e}}^*)\cdot\boldsymbol{\gamma}_{\mathrm{m}}\cdot(\hat{\boldsymbol{k}}\times\hat{\boldsymbol{e}})\right). \tag{3.3}$$

The integrated extinction (3.3) is based on the properties of the forward scattering dyadic $\mathbf{S}(k;-\hat{\boldsymbol{k}}\curvearrowright-\hat{\boldsymbol{k}})$ when viewed as a holomorphic function in the upper half of the complex k-plane. In particular, note that the right hand side of (3.3) is invariant when $\hat{\boldsymbol{e}}$ is replaced with $\hat{\boldsymbol{e}}^*$, implying that the integrated extinction is independent of the left- and right handed properties of the electric polarization.

Following the outline in Refs. 6 and 17, it is convenient to introduce the extinction volume ϱ as the complex-valued extension of the extinction cross section, *i.e.*,

$$\varrho(k;-\hat{\boldsymbol{k}},\hat{\boldsymbol{e}}^*) = \frac{\hat{\boldsymbol{e}}\cdot\mathbf{S}(k;-\hat{\boldsymbol{k}}\curvearrowright-\hat{\boldsymbol{k}})\cdot\hat{\boldsymbol{e}}^*}{k^2}. \tag{3.4}$$

This quantity defines a holomorphic function for $\operatorname{Im} k > 0$, and it is determined experimentally by a forward scattering measurement as discussed in Ref. 19. The extinction volume satisfies $\varrho(k; -\hat{\boldsymbol{k}}, \hat{\boldsymbol{e}}^*) = \varrho(k; -\hat{\boldsymbol{k}}, \hat{\boldsymbol{e}})$, meaning that also ϱ remains invariant when $\hat{\boldsymbol{e}}$ and $\hat{\boldsymbol{e}}^*$ are interchanged. For real-valued k, the extinction cross section is related to the imaginary part of extinction volume via the optical theorem

$$\sigma_{\text{ext}}(k; -\hat{\boldsymbol{k}}, \hat{\boldsymbol{e}}^*) = 4\pi k \operatorname{Im} \varrho(k; -\hat{\boldsymbol{k}}, \hat{\boldsymbol{e}}^*).$$

Analogous to the Kramers-Kronig relations on pp. 15–17 in Ref. 20, the real and imaginary parts of ϱ are connected by the Hilbert transform. In particular, it follows that ϱ is real-valued in the static limit and there satisfies the integral identity

$$\varrho(0; -\hat{\boldsymbol{k}}, \hat{\boldsymbol{e}}^*) = \frac{2}{\pi} \int_0^\infty \frac{\operatorname{Im} \varrho(k; -\hat{\boldsymbol{k}}, \hat{\boldsymbol{e}}^*)}{k} \, \mathrm{d}k. \tag{3.5}$$

Relation (3.5) is useful to check for consistency when ϱ is either measured or determined from a numerical calculation.

4 The three polarizability dyadics $\boldsymbol{\gamma}_{\text{e}}$, $\boldsymbol{\gamma}_{\text{m}}$ and $\boldsymbol{\gamma}_\infty$

Depending on the nature of the problem, let $\boldsymbol{\chi}_\ell$ denote either the electric ($\ell = \text{e}$) or magnetic ($\ell = \text{m}$) susceptibility dyadic in the static limit.[5] Assume that $\boldsymbol{\chi}_\ell$ is compactly supported and symmetric at all points $\boldsymbol{x} \in \mathbb{R}^3$. In the absence of a conductivity term, the electric and magnetic polarizability dyadics are defined by

$$\boldsymbol{\gamma}_\ell = \sum_{i,j=1}^{3} \left(\hat{\boldsymbol{a}}_i \cdot \iiint_{\mathbb{R}^3} \boldsymbol{\chi}_\ell(\boldsymbol{x}) \cdot (\hat{\boldsymbol{a}}_j - \nabla \psi_j(\boldsymbol{x})) \, \mathrm{dV} \right) \hat{\boldsymbol{a}}_i \hat{\boldsymbol{a}}_j, \tag{4.1}$$

where $\hat{\boldsymbol{a}}_1$, $\hat{\boldsymbol{a}}_2$ and $\hat{\boldsymbol{a}}_3$ form an arbitrary set of linearly independent unit vectors. Here, the scalar potential ψ_j is the unique solution of the static boundary value problem

$$\begin{cases} \nabla \cdot ((\boldsymbol{\chi}_\ell(\boldsymbol{x}) + \mathbf{I}_3) \cdot \nabla \psi_j(\boldsymbol{x})) = \nabla \cdot (\boldsymbol{\chi}_\ell(\boldsymbol{x}) \cdot \hat{\boldsymbol{a}}_i) \\ \psi_j(\boldsymbol{x}) = \mathcal{O}(x^{-2}) \text{ as } x \to \infty \end{cases} \qquad \boldsymbol{x} \in \mathbb{R}^3, \tag{4.2}$$

where $\mathbf{I}_3$ denotes the unit dyadic in $\mathbb{R}^3$. From (4.1) and (4.2) it is observed that $\boldsymbol{\gamma}_\ell$ merely is the induced dipole moment when the antenna is subject to an external electrostatic or magnetostatic excitation of unit amplitude. As a consequence, $\boldsymbol{\gamma}_\ell$ is independent of the direction of observation $\hat{\boldsymbol{k}}$ and the electric ($\ell = \text{e}$) or magnetic ($\ell = \text{m}$) polarization, $\hat{\boldsymbol{e}}$ and $\hat{\boldsymbol{k}} \times \hat{\boldsymbol{e}}$, respectively. Furthermore, from (4.1) and (4.2) it follows that $\boldsymbol{\gamma}_\ell$ is real-valued and symmetric since $\boldsymbol{\chi}_\ell$ is assumed to be symmetric at all points $\boldsymbol{x} \in \mathbb{R}^3$. Due to the absence of any length scale in the static limit, $\boldsymbol{\gamma}_\ell$ is proportional to the volume V occupied by the support

$$\Lambda = \{\boldsymbol{x} \in \mathbb{R}^3 \, : \, \boldsymbol{\chi}_{\text{e}}(\boldsymbol{x}) \neq \mathbf{0} \text{ or } \boldsymbol{\chi}_{\text{m}}(\boldsymbol{x}) \neq \mathbf{0}\},$$

[5] Here, $\boldsymbol{\chi}_{\text{e}} = \boldsymbol{\epsilon} - \mathbf{I}_3$ and $\boldsymbol{\chi}_{\text{m}} = \boldsymbol{\mu} - \mathbf{I}_3$, where $\boldsymbol{\epsilon}$ and $\boldsymbol{\mu}$ denote the static permittivity and permeability dyadics relative to free space, respectively.

see Ref. 17. Closed-form expressions of $\boldsymbol{\gamma}_\ell$ exist for various homogeneous and isotropic geometries, see Ref. 13 and references therein. Further discussions on the physical nature of $\boldsymbol{\gamma}_\ell$ are given on pp. 45–47 in Ref. 2 and pp. 63–65 in Ref. 21.[6]

From a modeling point of view it is also interesting to include a static conductivity in the susceptibility dyadic. For this purpose, assume that $\boldsymbol{\chi}_\ell$ is isotropic, *i.e.*, $\boldsymbol{\chi}_\ell = \chi_\ell \mathbf{I}_3$, and introduce the conductivity $\varsigma > 0$ and free space impedance $\eta_0 = \sqrt{\mu_0/\epsilon_0}$. In the presence of an isotropic conductivity term $\mathrm{i}\eta_0\varsigma/k$ in χ_ℓ, the pertinent definition of $\boldsymbol{\gamma}_\ell$ must be altered due to the singularity of the conductivity model in the static limit. Under this assumption, it follows from the discussion on pp. 49–51 in Ref. 13 that $\boldsymbol{\gamma}_\ell$ should be evaluated in the high-contrast limit as χ_ℓ approaches infinity. For this purpose, introduce the high-contrast polarizability dyadic $\boldsymbol{\gamma}_\infty$ via the limiting process $(i, j = 1, 2, 3)$

$$\hat{\boldsymbol{a}}_i \cdot \boldsymbol{\gamma}_\infty \cdot \hat{\boldsymbol{a}}_j = \lim_{\chi_\ell \to \infty} \hat{\boldsymbol{a}}_i \cdot \boldsymbol{\gamma}_\ell \cdot \hat{\boldsymbol{a}}_j, \tag{4.3}$$

where the dependence on χ_ℓ has been omitted on the right hand side of (4.3). Equivalently, the high-contrast polarizability dyadic is defined by

$$\boldsymbol{\gamma}_\infty = \sum_{i,j} \left(V + \hat{\boldsymbol{a}}_i \cdot \iint_{\partial\Lambda} \psi_j(\boldsymbol{x}) \hat{\boldsymbol{\nu}}(\boldsymbol{x}) - \boldsymbol{x} \hat{\boldsymbol{\nu}}(\boldsymbol{x}) \cdot (\hat{\boldsymbol{a}}_j + \nabla\psi_j(\boldsymbol{x})) \, \mathrm{dS} \right) \hat{\boldsymbol{a}}_i \hat{\boldsymbol{a}}_j, \tag{4.4}$$

where the surface integral is taken over the antenna boundary $\partial\Lambda$ with outward-directed unit normal vector $\hat{\boldsymbol{\nu}}$. Here, ψ_j is the solution to the exterior problem

$$\begin{cases} \nabla^2 \psi_j(\boldsymbol{x}) = 0 \\ \psi_j(\boldsymbol{x}) = -\hat{\boldsymbol{a}}_j \cdot \boldsymbol{x} + \mathcal{O}(x^{-2}) \text{ as } x \to \infty \end{cases} \qquad \boldsymbol{x} \in \mathbb{R}^3 \setminus \Lambda, \tag{4.5}$$

with the boundary condition of vanishing total charge, *i.e.*, $\int \hat{\boldsymbol{\nu}}(\boldsymbol{x}) \cdot \nabla\psi_j(\boldsymbol{x}) \, \mathrm{dS} = 0$, on each non-connected subset of $\partial\Lambda$.

5 Bounds on the integrated partial realized gain

A drawback of (2.2) is the presence of η on the right hand side of the identity. As mentioned in Sec. 3, the generalized absorption efficiency is determined from the overall scattering and absorption properties of the antenna. In contrast to the polarizability dyadics, η is not the solution of a pure electrostatic or magnetostatic problem. It is therefore important to observe that the following estimate directly can be invoked in the subsequent analysis:

$$0 \leq \eta(-\hat{\boldsymbol{k}}, \hat{\boldsymbol{e}}^*) < 1. \tag{5.1}$$

By introducing (5.1), the equality in (2.2) is turned into an inequality with an upper bound which solely is the solution an electrostatic and magnetostatic problem.

[6] Observe that the definition of $\boldsymbol{\gamma}_\ell$ in (4.1) deviates by a factor of 4π from Ref. 21.

In many cases, it is desirable to bound (2.2) from above independently of the materials in the antenna. This is achieved by introducing Jones' variational results, see Refs. 11 and 12, which are valid for general isotropic and heterogeneous material parameters. These variational results state that the eigenvalues of $\boldsymbol{\gamma}_\ell$ increase monotonically as χ_ℓ increases at any point $\boldsymbol{x} \in \mathbb{R}^3$. Hence, it follows from (4.3) that both $\boldsymbol{\gamma}_\mathrm{e}$ and $\boldsymbol{\gamma}_\mathrm{m}$ on the right hand side of (2.2) are bounded from above by $\boldsymbol{\gamma}_\infty$, *i.e.*,

$$\int_0^\infty \frac{g(k;\hat{\boldsymbol{k}},\hat{\boldsymbol{e}})}{k^4}\,\mathrm{d}k \leq \frac{\eta(-\hat{\boldsymbol{k}},\hat{\boldsymbol{e}}^*)}{2}\left(\hat{\boldsymbol{e}}^*\cdot\boldsymbol{\gamma}_\infty\cdot\hat{\boldsymbol{e}} + (\hat{\boldsymbol{k}}\times\hat{\boldsymbol{e}}^*)\cdot\boldsymbol{\gamma}_\infty\cdot(\hat{\boldsymbol{k}}\times\hat{\boldsymbol{e}})\right). \tag{5.2}$$

As a consequence, the parenthesis on the right hand side of (5.2) does not only hold for Λ, but also any extended support $\Lambda_+ \supset \Lambda$, meaning that $\boldsymbol{\gamma}_\infty$ can be estimated from above by the corresponding solution of (4.4) and (4.5) when Λ is replaced by Λ_+. This procedure is particular useful for estimating the high-contrast polarizability dyadic of a complicated antenna. In this case, the parenthesis on the right hand side of (5.2) is estimated from above by, for example, solving (4.4) and (4.5) for the smallest circumscribing cylinder with isotropic and homogeneous material parameters in the high-contrast limit.

The parenthesis on the right hand side of (5.2) is recognized as the Rayleigh quotients of $\boldsymbol{\gamma}_\infty$, implying that the integrated partial realized gain is further bounded from above by the eigenvalues of $\boldsymbol{\gamma}_\infty$. When subject to the constraint $\hat{\boldsymbol{e}}\cdot\hat{\boldsymbol{k}} = 0$ of transverse wave propagation, (5.2) implies

$$\int_0^\infty \frac{g(k;\hat{\boldsymbol{k}},\hat{\boldsymbol{e}})}{k^4}\,\mathrm{d}k \leq \frac{\eta(-\hat{\boldsymbol{k}},\hat{\boldsymbol{e}}^*)}{2}(\gamma_1+\gamma_2), \tag{5.3}$$

where γ_1 and γ_2 denote the largest and second largest eigenvalue of $\boldsymbol{\gamma}_\infty$, respectively. In the non-magnetic case, $(\hat{\boldsymbol{k}}\times\hat{\boldsymbol{e}}^*)\cdot\boldsymbol{\gamma}_\infty\cdot(\hat{\boldsymbol{k}}\times\hat{\boldsymbol{e}})$ and γ_2 vanish from the right hand sides of (5.2) and (5.3), respectively. For a discussion on the isoperimetric nature of the inequalities in (5.2) and (5.3), see Refs. 6 and 17.

As mentioned above, the right hand side of (2.2) can be estimated from above independently of the generalized absorption efficiency. By introducing (5.1) on the right hand side of (5.2), the upper bound on the integrated partial realized gain becomes independent of the $\hat{\boldsymbol{k}}$-direction, dependent only on the state of electric polarization $\hat{\boldsymbol{e}}$. Analogously, (5.1) inserted into the right hand side of (5.3) yields an upper bound which is independent of both $\hat{\boldsymbol{k}}$ and $\hat{\boldsymbol{e}}$. In the absence of any conductivity term in $\boldsymbol{\chi}_\ell$, bounds similar to (5.3) can also be derived for the eigenvalues of $\boldsymbol{\gamma}_\mathrm{e}$ and $\boldsymbol{\gamma}_\mathrm{m}$.

6 A priori estimates for UWB-antennas

A priori estimates for two archetypes of UWB-antennas are presented in this section, *viz.*, antennas characterized by a constant partial realized gain and antennas characterized by a constant effective antenna aperture. Generalizations of these models to more complex frequency characteristics are also addressed.

6.1 Constant partial realized gain $g_{\mathrm{p}}(\hat{\boldsymbol{k}}, \hat{\boldsymbol{e}})$

Due to the non-negative character of the partial realized gain, the left hand side of (2.2) can be estimated from below by integrating over $K = [k_{\mathrm{p}}, \infty)$ rather than the entire positive real axis. Thus, a straightforward calculation using the threshold $g_{\mathrm{p}}(\hat{\boldsymbol{k}}, \hat{\boldsymbol{e}}) = \min_{k \in K} g(k; \hat{\boldsymbol{k}}, \hat{\boldsymbol{e}})$ yields

$$\int_0^\infty \frac{g(k; \hat{\boldsymbol{k}}, \hat{\boldsymbol{e}})}{k^4} \, \mathrm{d}k \geq g_{\mathrm{p}}(\hat{\boldsymbol{k}}, \hat{\boldsymbol{e}}) \int_K \frac{\mathrm{d}k}{k^4} = \frac{g_{\mathrm{p}}(\hat{\boldsymbol{k}}, \hat{\boldsymbol{e}})}{3k_{\mathrm{p}}^3}. \tag{6.1}$$

Combining this estimate with (2.2) implies that

$$\frac{g_{\mathrm{p}}(\hat{\boldsymbol{k}}, \hat{\boldsymbol{e}})}{3k_{\mathrm{p}}^3} \leq \frac{\eta(-\hat{\boldsymbol{k}}, \hat{\boldsymbol{e}}^*)}{2} \left(\hat{\boldsymbol{e}}^* \cdot \boldsymbol{\gamma}_{\mathrm{e}} \cdot \hat{\boldsymbol{e}} + (\hat{\boldsymbol{k}} \times \hat{\boldsymbol{e}}^*) \cdot \boldsymbol{\gamma}_{\mathrm{m}} \cdot (\hat{\boldsymbol{k}} \times \hat{\boldsymbol{e}}) \right), \tag{6.2}$$

with equality if and only if $g(k; \hat{\boldsymbol{k}}, \hat{\boldsymbol{e}}) = g_{\mathrm{p}}(\hat{\boldsymbol{k}}, \hat{\boldsymbol{e}})$ for $k \in [k_{\mathrm{p}}, \infty)$, and zero elsewhere. The interpretation of (6.2) is that it yields a lower bound on the antenna onset frequency k_{p}, or, equivalently, an upper bound on the threshold $g_{\mathrm{p}}(\hat{\boldsymbol{k}}, \hat{\boldsymbol{e}})$, in terms of the geometry and static material parameters. From a physical point of view, an antenna with a constant partial realized gain is characterized by receiving less power as frequency increases since the effective antenna aperture (3.1) then varies inversely with the square of the frequency. Nearly self-complementary antennas such as the planar and conical equiangular spiral antennas are often modeled by a constant partial realized gain, see Sec. 7.

6.2 Constant effective antenna aperture $\pi g_{\mathrm{a}}(\hat{\boldsymbol{k}}, \hat{\boldsymbol{e}})/k_{\mathrm{a}}^2$

According to (3.1), a constant effective antenna aperture implies that the partial realized gain varies with the square of the frequency. For this purpose, introduce the constant effective antenna aperture $\pi g_{\mathrm{a}}(\hat{\boldsymbol{k}}, \hat{\boldsymbol{e}})/k_{\mathrm{a}}^2$, corresponding to the threshold $g_{\mathrm{a}}(\hat{\boldsymbol{k}}, \hat{\boldsymbol{e}}) = k_{\mathrm{a}}^2 \min_{k \in K} g(k; \hat{\boldsymbol{k}}, \hat{\boldsymbol{e}})/k^2$, where the frequency interval now is defined as $K = [k_{\mathrm{a}}, \infty)$. Then,

$$\int_0^\infty \frac{g(k; \hat{\boldsymbol{k}}, \hat{\boldsymbol{e}})}{k^4} \, \mathrm{d}k \geq \frac{g_{\mathrm{a}}(\hat{\boldsymbol{k}}, \hat{\boldsymbol{e}})}{k_{\mathrm{a}}^2} \int_K \frac{\mathrm{d}k}{k^2} = \frac{g_{\mathrm{a}}(\hat{\boldsymbol{k}}, \hat{\boldsymbol{e}})}{k_{\mathrm{a}}^3}.$$

Analogous to (6.2), it is concluded that

$$\frac{g_{\mathrm{a}}(\hat{\boldsymbol{k}}, \hat{\boldsymbol{e}})}{k_{\mathrm{a}}^3} \leq \frac{\eta(-\hat{\boldsymbol{k}}, \hat{\boldsymbol{e}}^*)}{2} \left(\hat{\boldsymbol{e}}^* \cdot \boldsymbol{\gamma}_{\mathrm{e}} \cdot \hat{\boldsymbol{e}} + (\hat{\boldsymbol{k}} \times \hat{\boldsymbol{e}}^*) \cdot \boldsymbol{\gamma}_{\mathrm{m}} \cdot (\hat{\boldsymbol{k}} \times \hat{\boldsymbol{e}}) \right), \tag{6.3}$$

with equality if and only if $g(k; \hat{\boldsymbol{k}}, \hat{\boldsymbol{e}}) = g_{\mathrm{a}}(\hat{\boldsymbol{k}}, \hat{\boldsymbol{e}}) k^2/k_{\mathrm{a}}^2$ for $k \in [k_{\mathrm{a}}, \infty)$, and zero elsewhere. Various horn and reflector antennas such as Hertz's parabolic cylinder on pp. 6–8 in Ref. 15 are examples of antennas with an approximately constant effective antenna aperture.

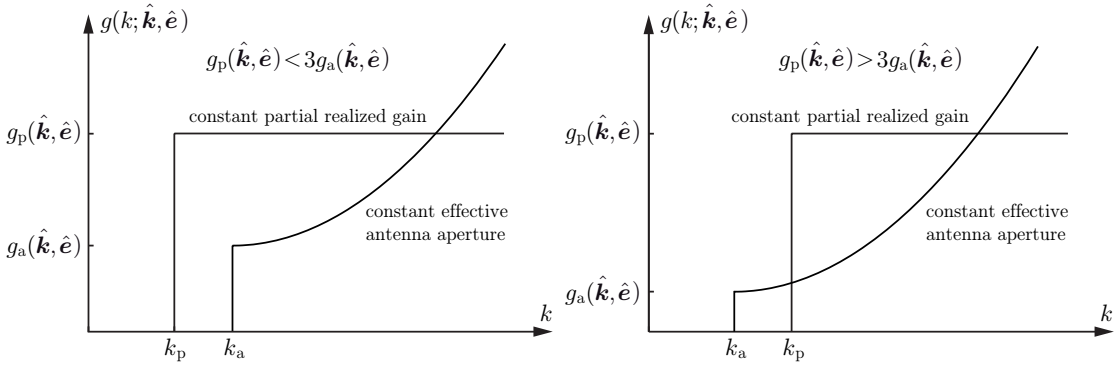

Figure 3: A comparison between the a priori estimates for a constant partial realized gain, $g_{\rm p}(\hat{\boldsymbol{k}},\hat{\boldsymbol{e}})$, and a constant effective antenna aperture, $\pi g_{\rm a}(\hat{\boldsymbol{k}},\hat{\boldsymbol{e}})/k_{\rm a}^2$.

For a given right hand side of (2.2), a comparison between (6.2) and (6.3) shows that the onset frequencies $k_{\rm p}$ and $k_{\rm a}$ satisfy

$$\frac{k_{\rm p}}{k_{\rm a}} = \left(\frac{g_{\rm p}(\hat{\boldsymbol{k}},\hat{\boldsymbol{e}})}{3g_{\rm a}(\hat{\boldsymbol{k}},\hat{\boldsymbol{e}})}\right)^{1/3},$$

implying that $k_{\rm p} > k_{\rm a}$ for $g_{\rm p}(\hat{\boldsymbol{k}},\hat{\boldsymbol{e}}) > 3g_{\rm a}(\hat{\boldsymbol{k}},\hat{\boldsymbol{e}})$, and $k_{\rm p} < k_{\rm a}$ for $g_{\rm p}(\hat{\boldsymbol{k}},\hat{\boldsymbol{e}}) < 3g_{\rm a}(\hat{\boldsymbol{k}},\hat{\boldsymbol{e}})$. This conclusion is illustrated in Fig. 3 using the following models with identical values of the integrated partial realized gain (2.2): $g(k;\hat{\boldsymbol{k}},\hat{\boldsymbol{e}}) = g_{\rm p}(\hat{\boldsymbol{k}},\hat{\boldsymbol{e}})$ for $k \in [k_{\rm p},\infty)$, and $g(k;\hat{\boldsymbol{k}},\hat{\boldsymbol{e}}) = g_{\rm a}(\hat{\boldsymbol{k}},\hat{\boldsymbol{e}})k^2/k_{\rm a}^2$ for $k \in [k_{\rm a},\infty)$, and zero elsewhere. In particular, the orderings $g_{\rm p}(\hat{\boldsymbol{k}},\hat{\boldsymbol{e}}) < 3g_{\rm a}(\hat{\boldsymbol{k}},\hat{\boldsymbol{e}})$ and $g_{\rm p}(\hat{\boldsymbol{k}},\hat{\boldsymbol{e}}) > 3g_{\rm a}(\hat{\boldsymbol{k}},\hat{\boldsymbol{e}})$ in Fig. 3 refer to the onset frequencies $k_{\rm p} < k_{\rm a}$ and $k_{\rm p} > k_{\rm a}$, respectively. Of course, it is unphysical to include infinite high frequencies in the models, but it is not a severe restriction since the damping factor $1/k^4$ implies that the integrated partial realized gain (2.2) is dominated by the antenna's low- and intermediate frequency behavior.

6.3 More general models of UWB-antennas

Although many UWB-antennas may be characterized as having a constant partial realized gain or a constant effective antenna aperture, there are also antennas that do not fall into this classification. In fact, the UWB-antenna is only one part of a broadband communication system designed to meet an overall specification. It is therefore motivated to briefly discuss more general models of UWB-antennas based on the analysis of the lossy transmission problem on pp. 191–193 in Ref. 4. From that analysis it is clear that the low-frequency behavior of the effective antenna aperture is governed by $\sigma_{\rm a}(k;\hat{\boldsymbol{k}},\hat{\boldsymbol{e}}) = \mathcal{O}(k^2)$ as $k \to 0$, or equivalently,

$$g(k;\hat{\boldsymbol{k}},\hat{\boldsymbol{e}}) = \mathcal{O}(k^4) \text{ as } k \to 0, \tag{6.4}$$

where (3.1) has been used. Relation (6.4) is a natural choice of low-frequency behavior to guarantee the existence of (2.2) in the classical sense. Instead of choosing

a constant partial realized gain or a constant effective antenna aperture, which obviously lacks any continuity properties at $k = k_{\mathrm{p}}$ and $k = k_{\mathrm{a}}$, each antenna designer may choose her own model to fulfill the system requirements. Then, based on this model, the antenna onset frequency is determined by simply solving an electrostatic or magnetostatic problem as emphasized in Sec. 4.

6.4 A numerical example for the circular disk

As an example of how the theoretical findings in Secs. 5 and 6 can be used in modern antenna design, consider an arbitrary planar antenna Λ circumscribed by a circular disk Λ_+ of radius a. Let $\hat{\boldsymbol{\nu}}$ denote the outward-directed unit normal vector of the disk, and choose $\hat{\boldsymbol{k}} = \hat{\boldsymbol{\nu}}$ and $\hat{\boldsymbol{e}} = \hat{\boldsymbol{\rho}}$, where $\hat{\boldsymbol{\rho}}$ denotes the radial unit vector in polar coordinates. This choice of $\hat{\boldsymbol{k}}$ and $\hat{\boldsymbol{e}}$ correspond to a direction of observation and an electric polarization which are perpendicular and parallell to the disk, respectively. Introduce the UWB frequency band $f \in [3.1, 10.6]\,\mathrm{GHz}$, or equivalently $k \in [0.65, 2.22]\,\mathrm{cm}^{-1}$, as briefly mentioned in Sec. 1. Assume that Λ is specified to have a partial realized gain

$$g(k; \hat{\boldsymbol{\nu}}, \hat{\boldsymbol{\rho}}) \geq \begin{cases} g_{\mathrm{level}}(\hat{\boldsymbol{\nu}}, \hat{\boldsymbol{\rho}}) k^4/k_1^4 & k \in [0, k_1] \\ g_{\mathrm{level}}(\hat{\boldsymbol{\nu}}, \hat{\boldsymbol{\rho}}) & k \in [k_1, k_2] \\ 0 & \text{otherwise} \end{cases} \tag{6.5}$$

where $k_1 = 0.65\,\mathrm{cm}^{-1}$ and $k_2 = 2.22\,\mathrm{cm}^{-1}$. Then, for a given threshold $g_{\mathrm{level}}(\hat{\boldsymbol{\nu}}, \hat{\boldsymbol{\rho}})$, it is desirable to determine the smallest radius a such that it is feasible for $\Lambda \subset \Lambda_+$ to have a partial realized gain satisfying (6.5).

Based on the specification in (6.5), a straightforward calculation of (2.2) yields

$$\int_0^\infty \frac{g(k; \hat{\boldsymbol{\nu}}, \hat{\boldsymbol{\rho}})}{k^4}\,\mathrm{d}k \geq g_{\mathrm{level}}(\hat{\boldsymbol{\nu}}, \hat{\boldsymbol{\rho}}) \left(\frac{1}{k_1^3} + \int_{k_1}^{k_2} \frac{\mathrm{d}k}{k^4} \right) = \frac{g_{\mathrm{level}}(\hat{\boldsymbol{\nu}}, \hat{\boldsymbol{\rho}})}{3} \frac{4k_2^3 - k_1^3}{k_1^3 k_2^3}. \tag{6.6}$$

From the analysis in Ref. 17, it follows that the electric and magnetic polarizability dyadics of the perfectly electric conducting circular disk are $\boldsymbol{\gamma}_{\mathrm{e}} = 16a^3\mathbf{I}_\perp/3$ and $\boldsymbol{\gamma}_{\mathrm{m}} = \mathbf{0}$, where $\mathbf{I}_\perp = \mathbf{I}_3 - \hat{\boldsymbol{\nu}}\hat{\boldsymbol{\nu}}$ is the projection dyadic in $\mathbb{R}^3$. Hence, by inserting (6.6) into (2.2), one obtain

$$\frac{g_{\mathrm{level}}(\hat{\boldsymbol{\nu}}, \hat{\boldsymbol{\rho}})}{a^3} \leq 0.55\eta(-\hat{\boldsymbol{\nu}}, \hat{\boldsymbol{\rho}}), \tag{6.7}$$

where a now measures the radius of the disk in units of cm. For example, by invoking the upper bound in (5.1), it is concluded that the minimum radius of the disk is 1.8 cm for $g_{\mathrm{level}}(\hat{\boldsymbol{\nu}}, \hat{\boldsymbol{\rho}}) = 3$ and 1.9 cm for $g_{\mathrm{level}}(\hat{\boldsymbol{\nu}}, \hat{\boldsymbol{\rho}}) = 4$. For many antennas, η is close to $1/2$ and a more realistic bound is therefore 2.2 cm and 2.4 cm for $g_{\mathrm{level}}(\hat{\boldsymbol{\nu}}, \hat{\boldsymbol{\rho}}) = 3$ and $g_{\mathrm{level}}(\hat{\boldsymbol{\nu}}, \hat{\boldsymbol{\rho}}) = 4$, respectively. Finally, note that various planar antennas directly can be compared with (6.7) to establish measures of how effective they make use of their surface areas.

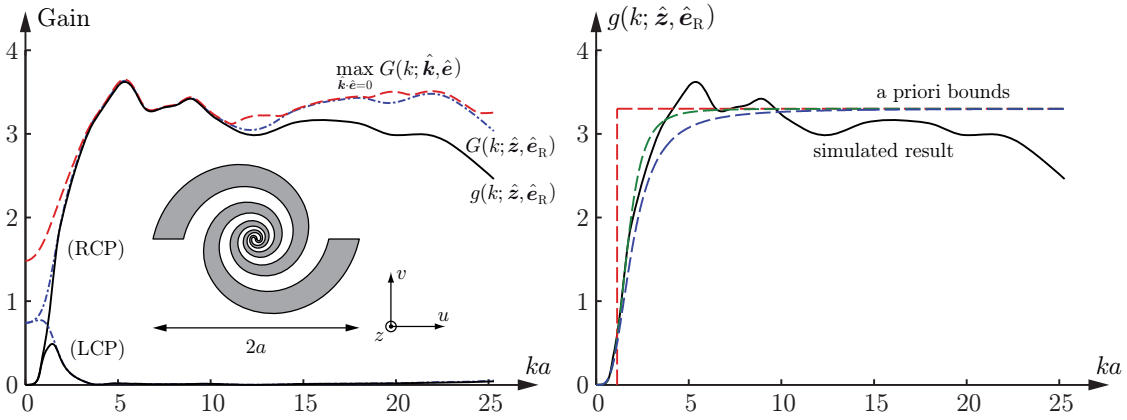

Figure 4: Left figure: maximum gain, $\max_{\hat{\boldsymbol{k}}\cdot\hat{\boldsymbol{e}}=0} G(k;\hat{\boldsymbol{k}},\hat{\boldsymbol{e}})$ (red dashed line), partial gain $G(k;\hat{\boldsymbol{z}},\cdot)$ (blue dashed-dotted line), and partial realized gain $g(k;\hat{\boldsymbol{z}},\cdot)$ (black solid line) for both the $\hat{\boldsymbol{e}}_{\mathrm{R}}$- and $\hat{\boldsymbol{e}}_{\mathrm{L}}$-polarizations. Right figure: a priori estimates of $g(k;\hat{\boldsymbol{z}},\hat{\boldsymbol{e}}_{\mathrm{R}})$ derived from electrostatic properties of the antenna using $\eta_{\mathrm{R}} = 0.62$.

7 The equiangular planar spiral antenna

In this section, numerical results for the equiangular planar spiral antenna is presented and compared with the estimates introduced in Secs. 5 and 6.

7.1 General properties

Dyson's equiangular planar spiral antenna in Fig. 4 is an example of a nearly self-complementary antenna often modeled by a constant partial realized gain. It is parameterized by the azimuthal angle ϕ in terms of four radial distances according to Ref. 5. In terms of $\vartheta = 5/4$ and the radius a of the smallest circumscribing disk, the parameterizations of the two spiral arms are $r_1(\phi) = a\vartheta^{\phi-4\pi}$ and $r_2(\phi) = a\vartheta^{\phi-9\pi/2}$ for $\phi \in [0, 4\pi]$, and $r_3(\phi) = a\vartheta^{\phi-5\pi}$ and $r_4(\phi) = a\vartheta^{\phi-11\pi/2}$ for $\phi \in [\pi, 5\pi]$. Introduce the coordinate system $(\hat{\boldsymbol{u}}, \hat{\boldsymbol{v}}, \hat{\boldsymbol{z}})$ with the $\hat{\boldsymbol{z}}$-axis being outward-directed from the plane of the antenna. Then, according to the IEEE-standard in Ref. 1, the transmitted waves from the antenna result in right-circularly polarized (RCP or $\hat{\boldsymbol{e}}_{\mathrm{R}}$-polarized) radiation in the positive $\hat{\boldsymbol{z}}$-direction, and thus left-circularly polarized (LCP or $\hat{\boldsymbol{e}}_{\mathrm{L}}$-polarized) radiation in the negative $\hat{\boldsymbol{z}}$-direction. The electric polarizations $\hat{\boldsymbol{e}}_{\mathrm{R}}$ and $\hat{\boldsymbol{e}}_{\mathrm{L}}$ are related by $\hat{\boldsymbol{e}}_{\mathrm{R}}^* = \hat{\boldsymbol{e}}_{\mathrm{L}}$, where

$$\begin{cases} \hat{\boldsymbol{e}}_{\mathrm{R}} = \frac{1}{\sqrt{2}}(\hat{\boldsymbol{u}} + \mathrm{i}\hat{\boldsymbol{v}}) & (\mathrm{RCP}) \\ \hat{\boldsymbol{e}}_{\mathrm{L}} = \frac{1}{\sqrt{2}}(\hat{\boldsymbol{u}} - \mathrm{i}\hat{\boldsymbol{v}}) & (\mathrm{LCP}) \end{cases}, \qquad \begin{cases} \hat{\boldsymbol{e}}_{\mathrm{R}} = \frac{1}{\sqrt{2}}(\hat{\boldsymbol{u}} - \mathrm{i}\hat{\boldsymbol{v}}) & (\mathrm{RCP}) \\ \hat{\boldsymbol{e}}_{\mathrm{L}} = \frac{1}{\sqrt{2}}(\hat{\boldsymbol{u}} + \mathrm{i}\hat{\boldsymbol{v}}) & (\mathrm{LCP}) \end{cases},$$

for radiation in the positive and negative $\hat{\boldsymbol{z}}$-directions, respectively. Here, the partial realized gain satisfies $g(k;\hat{\boldsymbol{z}},\hat{\boldsymbol{e}}) = g(k;-\hat{\boldsymbol{z}},\hat{\boldsymbol{e}}^*)$, where $\hat{\boldsymbol{e}}$ denotes any of $\hat{\boldsymbol{e}}_{\mathrm{R}}$ and $\hat{\boldsymbol{e}}_{\mathrm{L}}$. As a consequence, it is sufficient to only treat the radiation in the positive $\hat{\boldsymbol{z}}$-direction.

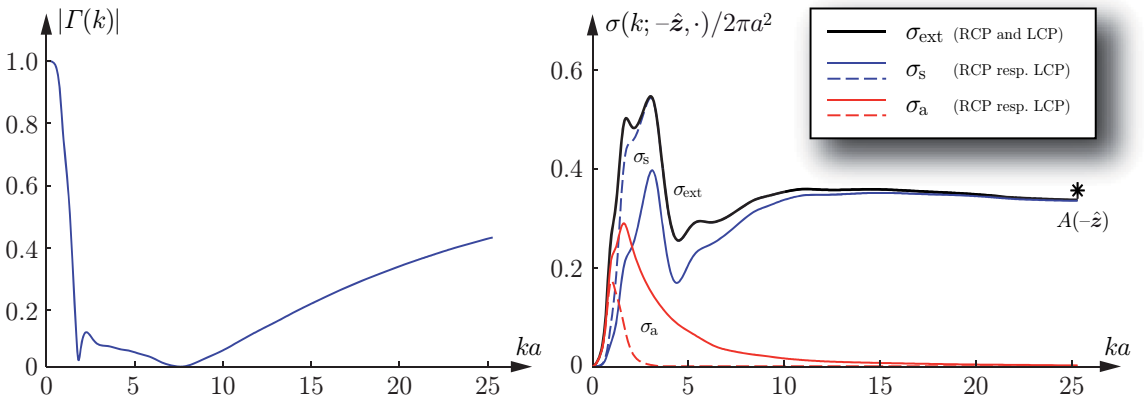

Figure 5: Left figure: the magnitude of the reflection coefficient Γ matched to the input impedance $250\,\Omega$. Right figure: the extinction cross section, scattering cross section and effective antenna aperture, $\sigma_{\rm ext}$, $\sigma_{\rm s}$, and $\sigma_{\rm a}$, respectively, in units of $2\pi a^2$.

7.2 Numerical results

A numerical solution of the Maxwell equations using the commercial EFIELD method of moments solver[7] is employed to illustrate the estimates in Secs. 5 and 6. For this purpose, the equiangular planar spiral antenna is modeled by perfectly electric conducting material and matched to the input impedance $250\,\Omega$. It is simulated using a delta gap feed model and the resulting reflection coefficient Γ is depicted on the left hand side of Fig. 5. Based on the voltage standing wave ratio VSWR ≤ 2, or equivalently, $|\Gamma| \leq 1/3$, the bandwidth of the equiangular planar spiral antenna is calculated to be 171% relative to the center frequency $k_0 a = 10.5$. The maximum gain, $G_{\rm max}(k) = \max_{\hat{\boldsymbol{k}}\cdot\hat{\boldsymbol{e}}=0} G(k;\hat{\boldsymbol{k}},\hat{\boldsymbol{e}})$, the partial gain $G(k;\hat{\boldsymbol{z}},\cdot)$ in the positive $\hat{\boldsymbol{z}}$-direction, and the partial realized gain $g(k;\hat{\boldsymbol{z}},\cdot)$ in the positive $\hat{\boldsymbol{z}}$-direction are depicted on the left hand side of Fig. 4. It is observed that $g(k;\hat{\boldsymbol{z}},\hat{\boldsymbol{e}}_{\rm R})$ is approximately constant over a large frequency interval with a main beam in the positive $\hat{\boldsymbol{z}}$-direction. For comparison, the corresponding results for the LCP-radiation are included in Fig. 4 with an overall partial realized gain $g(k;\hat{\boldsymbol{z}},\hat{\boldsymbol{e}}_{\rm L})$ less than unity.

The equiangular spiral antenna is also simulated in plane wave scattering when it is loaded with $250\,\Omega$ in parallel with the feeding port. The resulting extinction cross section, scattering cross section, and effective antenna aperture, are depicted on the right hand side of Fig. 5.[8] It is seen that that the scattering effects are dominant when the impinging plane wave is $\mathrm{e}^{-\mathrm{i}k\hat{\boldsymbol{z}}\cdot\boldsymbol{x}}\hat{\boldsymbol{e}}_{\rm R}$, while the absorption properties are more noticeable for the excitation $\mathrm{e}^{-\mathrm{i}k\hat{\boldsymbol{z}}\cdot\boldsymbol{x}}\hat{\boldsymbol{e}}_{\rm L}$. The high-frequency limit $A(-\hat{\boldsymbol{z}}) = 0.36$ of the extinction cross section is marked by a star in Fig. 5. In fact, according to the

[7] More information about this code is available at http://www.efieldsolutions.com.

[8] The notations (RCP) and (LCP) in Figs. 5 and 6 refer to the polarization of the antenna rather than the incident wave, *i.e.*, (RCP) and (LCP) should be interpreted as an incident plane being left- and right-circularly polarized, respectively.

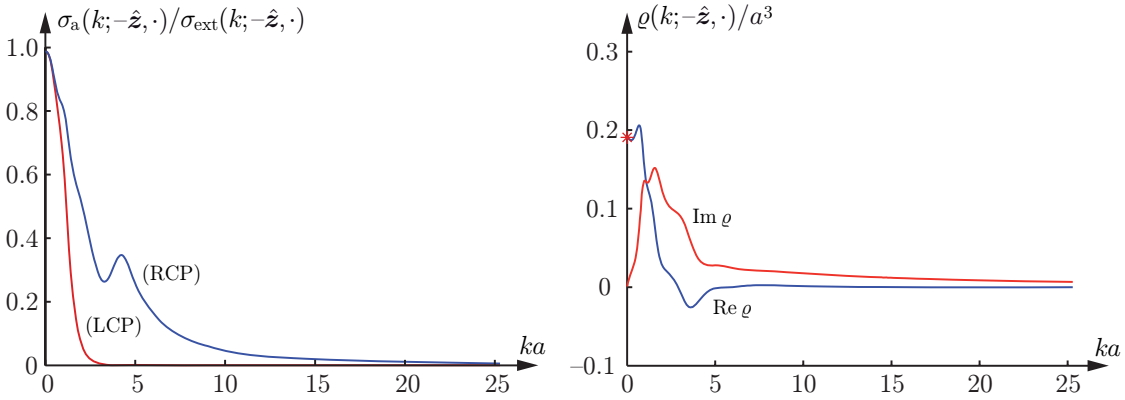

Figure 6: The pointwise absorption efficiency σ_a/σ_{ext} (left figure), and the real and imaginary parts of the extinction volume ϱ in units of a^3 (right figure).

extinction paradox in Ref. 17,

$$\lim_{k\to\infty} \sigma_{ext}(k;-\hat{\boldsymbol{z}},\cdot) = 2\pi a^2 A(-\hat{\boldsymbol{z}}),$$

where A denotes the projected area of the antenna in units of πa^2. The corresponding curves for the pointwise absorption efficiency σ_a/σ_{ext} and the extinction volume ϱ are illustrated in Fig. 6. Recall that the extinction volume is identical for both the $\hat{\boldsymbol{e}}_R$- and $\hat{\boldsymbol{e}}_L$-polarizations. In particular, the star on the right hand side of Fig. 6 indicate the value of the integral on the right hand side of (3.5). So, for the equiangular planar spiral antenna in Fig. 4 it is concluded that the integral identity (3.5) holds.

The general absorption efficiency is calculated from the integrated absorption and integrated extinction in (3.2). The result is $\eta_R = 0.62$ and $\eta_L = 0.40$, where $\eta_R = \eta(-\hat{\boldsymbol{z}}, \hat{\boldsymbol{e}}_R^*)$ and $\eta_L = \eta(-\hat{\boldsymbol{z}}, \hat{\boldsymbol{e}}_L^*)$ following the notation in Sec. 3. This observation implies that the quotients $\eta_R/(\eta_R+\eta_L) = 0.61$ and $\eta_L/(\eta_R+\eta_L) = 0.39$ may be interpreted as quality factors for the antenna's overall ability to intercept any of the two polarizations.

7.3 Analysis of the electric polarizability dyadic

The electric polarizability dyadic of the antenna is calculated by numerically solving (4.2) in the perfectly electric conducting limit. Expressed in the basis $(\hat{\boldsymbol{u}}, \hat{\boldsymbol{v}}, \hat{\boldsymbol{z}})$, the dyadic reduces to the symmetric matrix

$$[\boldsymbol{\gamma}_e] = \begin{pmatrix} 2.82 & -0.63 & 0 \\ -0.63 & 1.98 & 0 \\ 0 & 0 & 0 \end{pmatrix} a^3. \tag{7.1}$$

The corresponding magnetic polarizability matrix vanishes, *i.e.*, $[\boldsymbol{\gamma}_m] = \boldsymbol{0}$, since no induced magnetic dipole moment is supported by the antenna. In particular, note that the elements in the third row and third column in (7.1) are identically zero,

reflecting the vanishing thickness of the antenna in the $\hat{\boldsymbol{z}}$-direction. The largest eigenvalue $\gamma_1 = 3.16a^3$ should be compared with the corresponding number $16a^3/3$ for the smallest circumscribing disk with isotropic and homogeneous material parameters in the high-contrast limit. Having Jones' variational results from Sec. 5 in mind, the value $16a^3/3$, or approximately $5.33a^3$, is a priori known to be an upper bound on γ_1. Although the equiangular planar spiral antenna only occupies 36% of the smallest circumscribing disk (recall that $A(-\hat{\boldsymbol{z}}) = 0.36$), this antenna makes effective use of its surface area since

$$\zeta = \frac{\gamma_1}{\pi a^2 A(-\hat{\boldsymbol{z}})} = 2.79a. \tag{7.2}$$

The surface area efficiency (7.2) should be compared with the corresponding number $1.70a$ if the entire circular disk is used as an antenna.

The first Rayleigh quotient on right hand side of (2.2) is obtained from (7.1) by a straightforward matrix multiplication, *viz.*,

$$\hat{\boldsymbol{e}}^* \cdot [\boldsymbol{\gamma}_{\mathrm{e}}] \cdot \hat{\boldsymbol{e}} = \frac{1}{2} \begin{pmatrix} 1 \\ \pm \mathrm{i} \\ 0 \end{pmatrix}^{\dagger} \begin{pmatrix} 2.82 & -0.63 & 0 \\ -0.63 & 1.98 & 0 \\ 0 & 0 & 0 \end{pmatrix} \begin{pmatrix} 1 \\ \pm \mathrm{i} \\ 0 \end{pmatrix} a^3 = 2.40a^3, \tag{7.3}$$

where a dagger denotes the complex conjugate transpose, and the upper and lower signs in (7.3) refer to $\hat{\boldsymbol{e}} = \hat{\boldsymbol{e}}_{\mathrm{R}}$ and $\hat{\boldsymbol{e}} = \hat{\boldsymbol{e}}_{\mathrm{L}}$, respectively.[9] The result in (7.3) should also be compared with the corresponding value $5.33a^3$ for the smallest circumscribing disk. Both $3.16a^3$ and $5.33a^3$ yield upper bounds on the integrated partial realized gain when inserted into the right hand side of (5.3). For this purpose, recall that γ_2 vanishes from the left hand side of (5.3) since the magnetic polarizability matrix is identically zero.

7.4 A priori estimates of the partial realized gain

Without loss of generality, let $\hat{\boldsymbol{e}} = \hat{\boldsymbol{e}}_{\mathrm{R}}$ and $\eta = \eta_{\mathrm{R}}$ throughout this section. Further, introduce the scaled partial realized gain $f(\kappa) = g(k; \hat{\boldsymbol{z}}, \hat{\boldsymbol{e}}_{\mathrm{R}})$, where $\kappa = ka$. Then, (2.2) implies

$$\int_0^\infty \frac{g(k)}{k^4}\, \mathrm{d}k = a^3 \int_0^\infty \frac{f(\kappa)}{\kappa^4}\, \mathrm{d}\kappa = \frac{\eta_{\mathrm{R}}}{2}\Big(\hat{\boldsymbol{e}}_{\mathrm{R}}^* \cdot \boldsymbol{\gamma}_{\mathrm{e}} \cdot \hat{\boldsymbol{e}}_{\mathrm{R}} + (\hat{\boldsymbol{z}} \times \hat{\boldsymbol{e}}_{\mathrm{R}}^*) \cdot \boldsymbol{\gamma}_{\mathrm{m}} \cdot (\hat{\boldsymbol{z}} \times \hat{\boldsymbol{e}}_{\mathrm{R}})\Big).$$

Equivalently, by invoking (7.3) and $\eta = 0.62$, one obtain the following integral independent of the radius a of the smallest circumscribing disk:

$$\int_0^\infty \frac{f(\kappa)}{\kappa^4}\, \mathrm{d}\kappa = 0.74, \tag{7.4}$$

Any function f satisfying (7.4) with the low-frequency behavior $f(\kappa) = \mathcal{O}(\kappa^4)$ as $\kappa \to 0$ is a possible candidate for a partial realized gain of the equiangular spiral

[9] Recall that (7.3) is independent of the left- and right-handed properties of the polarization since $[\boldsymbol{\gamma}_{\mathrm{e}}]$ is symmetric.

antenna. Additional knowledge or specification of the performance of the antenna must then be invoked to further establish a priori estimates on the partial realized gain. For example, consider the model $f(\kappa) = 3.3$ for $\kappa \in [\kappa_{\mathrm{p}}, \infty)$, and zero elsewhere. This model is illustrated by the uppermost dashed line in Fig. 4. The onset frequency $\kappa_{\mathrm{p}} = k_{\mathrm{p}}a$ of this bound is then given by (6.2), *i.e.*,

$$\kappa_{\mathrm{p}} \geq \left(\frac{3.3}{3 \cdot 0.74}\right)^{1/3} = 1.14.$$

A more realistic model of the partial realized gain is $f(\kappa) = g_{\mathrm{level}}\kappa^4/(\alpha + \kappa^4)$, where the constant α satisfies the integral equation

$$\int_0^\infty \frac{f(\kappa)}{\kappa^4}\, \mathrm{d}\kappa = g_{\mathrm{level}} \int_0^\infty \frac{\mathrm{d}\kappa}{\alpha + \kappa^4} = \frac{2.40 \cdot 0.62}{2} = 0.74. \tag{7.5}$$

A numerical solution of (7.5) yields $\alpha = 8.40$, implying that $f(\kappa) = 3.3\kappa^4/(8.40+\kappa^4)$ is a potential estimate of the partial realized gain. This estimate is illustrated by the intervening dashed line in Fig. 4. Finally, a somewhat different bound is obtained using $f(\kappa) = g_{\mathrm{level}}\kappa^4/(\beta + \kappa^{8/3})^{3/2}$, where the constant β is given by

$$\int_0^\infty \frac{f(\kappa)}{\kappa^4}\, \mathrm{d}\kappa = g_{\mathrm{level}} \int_0^\infty \frac{\mathrm{d}\kappa}{(\beta + \kappa^{8/3})^{3/2}} = \frac{2.40 \cdot 0.62}{2} = 0.74. \tag{7.6}$$

A numerical solution of (7.6) yields $\beta = 3.58$, and this estimate is illustrated by the lowermost dashed line in Fig. 4. Note that the three estimates above satisfy the correct low-frequency behavior (6.4).

8 Conclusions

In this paper, a summation rule valid for a large class of linear and reciprocal antennas is presented. In particular, a priori estimates on the partial realized gain and antenna onset frequency are derived for two important archetypes of UWB-antennas: those with a constant partial realized gain, and those with a constant effective antenna aperture. These estimates are numerically exemplified in Secs. 6 and 7 by the smallest circumscribing disk and the equiangular planar spiral antenna, respectively. Although the electric and magnetic polarizability dyadics are restricted to the static or long wavelength limit, the above-mentioned examples suggest that the polarizability dyadics are crucial for the understanding of an antenna's ability to direct or focus energy over a frequency interval. For example, from (4.4) and (4.5) it is clear that the high-contrast polarizability dyadic is defined as the first moment of the induced charge density. As a consequence, the further the accumulated charges are separated by an external applied field, the larger is the corresponding elements of the polarizability dyadic. Another striking consequence of (4.4) and (4.5) is that the interior of an antenna has less influence on the polarizability dyadic than the antenna's boundary surface. Removing interior parts of the antenna will only slightly reduce the integrated partial realized gain (2.2), but mainly redistribute

the integrand along the frequency axis. It is thus concluded that the high-contrast polarizability dyadic reproduces and quantifies the well known rule of thumb that the boundary is the critical parameter in antenna design, far more so than its surface area or interior geometry.

The estimates introduced in this paper are also valuable for comparing existing antenna designs with various circumscribing geometries. Such a comparison implies that antennas can be classified in terms of its surface or volume efficiency, *cf.*, the discussion in Sec. 6.4. Of course, the polarizability dyadics do not completely determine the antenna performance. For example, the polarizability dyadics are ignorant of whether it is advantageous to model a given structure as a resonant antenna or as an antenna having a broadband frequency characteristic.

Acknowledgment

The financial support by the Swedish Research Council and the SSF Center for High Speed Wireless Communication is gratefully acknowledged. The authors are also grateful for fruitful discussions with Anders Karlsson at the Department of Electrical and Information Technology, Lund University, Sweden.

References

[1] Antenna Standards Committee of the IEEE Antennas and Propagation Society. IEEE Standard Definitions of Terms for Antennas, 1993. IEEE Std 145-1993.

[2] S. Chandrasekhar. *Radiative Transfer*. Dover Publications, New York, 1960.

[3] L. J. Chu. Physical limitations of omni-directional antennas. *Appl. Phys.*, **19**, 1163–1175, 1948.

[4] G. Dassios and R. Kleinman. *Low frequency scattering*. Oxford University Press, Oxford, 2000.

[5] J. Dyson. The equiangular spiral antenna. *IEEE Trans. Antennas Propagat.*, **7**(2), 181–187, 1959.

[6] M. Gustafsson, C. Sohl, and G. Kristensson. Physical limitations on antennas of arbitrary shape. *Proc. R. Soc. A*, **463**, 2589–2607, 2007.

[7] M. Gustafsson, C. Sohl, and G. Kristensson. Physical limitations on scattering and absorption of antennas. In *Proceedings of the Second European Conference on Antennas and Propagation*. The Institution of Engineering and Technology, 2007.

[8] M. Gustafsson, C. Sohl, and G. Kristensson. Physical limitations on antennas of arbitrary shape. Technical Report LUTEDX/(TEAT-7153)/1–37/(2007), Lund University, Department of Electrical and Information Technology, P.O. Box 118, S-221 00 Lund, Sweden, 2007. http://www.eit.lth.se.

[9] R. C. Hansen. *Electrically small, superdirective, and superconductive antennas.* John Wiley & Sons, New Jersey, 2006.

[10] A. Hujanen, J. Holmberg, and J. C.-E. Sten. Bandwidth limitations of impedance matched ideal dipoles. *IEEE Trans. Antennas Propagat.*, **53**(10), 3236–3239, 2005.

[11] D. S. Jones. Low frequency electromagnetic radiation. *J. Inst. Maths. Applics.*, **23**(4), 421–447, 1979.

[12] D. S. Jones. Scattering by inhomogeneous dielectric particles. *Quart. J. Mech. Appl. Math.*, **38**, 135–155, 1985.

[13] R. E. Kleinman and T. B. A. Senior. Rayleigh scattering. In V. V. Varadan and V. K. Varadan, editors, *Low and high frequency asymptotics*, volume 2 of *Handbook on Acoustic, Electromagnetic and Elastic Wave Scattering*, chapter 1, pages 1–70. Elsevier Science Publishers, Amsterdam, 1986.

[14] R. G. Newton. *Scattering Theory of Waves and Particles.* Dover Publications, New York, second edition, 2002.

[15] H. Schantz. *The Art and Science of Ultrawideband Antennas.* Artech House, Boston, London, 2005.

[16] S. Silver. *Microwave Antenna Theory and Design*, volume 12 of *Radiation Laboratory Series.* McGraw-Hill, New York, 1949.

[17] C. Sohl, M. Gustafsson, and G. Kristensson. Physical limitations on broadband scattering by heterogeneous obstacles. *J. Phys. A: Math. Theor.*, **40**, 11165–11182, 2007.

[18] C. Sohl, M. Gustafsson, and G. Kristensson. Physical limitations on metamaterials: Restrictions on scattering and absorption over a frequency interval. *J. Phys. D: Applied Phys.*, **40**, 7146–7151, 2007.

[19] C. Sohl, C. Larsson, M. Gustafsson, and G. Kristensson. A scattering and absorption identity for metamaterials: experimental results and comparison with theory. Accepted for publication in J. Appl. Phys., 2007.

[20] C. Sohl. *Dispersion Relations for Extinction of Acoustic and Electromagnetic Waves.* Licentiate thesis, Lund University, Department of Electrical and Information Technology, P.O. Box 118, S-221 00 Lund, Sweden, 2007. http://www.eit.lth.se.

[21] H. van de Hulst. *Light Scattering by Small Particles.* John Wiley & Sons, Inc., New York, 1957.

[22] M. C. Villalobos, H. D. Foltz, J. S. McLean, and I. Sen Gupta. Broadband tuning limits on UWB antennas based on Fano's formulation. In C. E. Baum, A. P. Stone, and J. S. Tyo, editors, *Ultra-Wideband, Short-Pulse Electromagnetics 8*, pages 83–87. Springer-Verlag, New York, 2007.

[23] H. A. Wheeler. Fundamental limitations of small antennas. *Proc. IRE*, **35**(12), 1479–1484, 1947.